Scientific Research Publishing

Optics and Photonics Journal, 2023, 13, 119-132
https://www.scirp.org/journal/opj
ISSN Online: 2160-889X
ISSN Print: 2160-8881

A High Spectral Efficient Frequency-Domain Channel-Estimation Method for the Polarization-Division-Multiplexed CO-OFDM-OQAM System

Hangyu Zhao, Shuo Zhang, Daobin Wang*, Xiaoxiao Li, Lihua Yuan

School of Science, Lanzhou University of Technology, Lanzhou, China
Email: *cougarlz@lut.edu.cn

How to cite this paper: Zhao, H.Y., Zhang, S., Wang, D.B., Li, X.X. and Yuan, L.H. (2023) A High Spectral Efficient Frequency-Domain Channel-Estimation Method for the Polarization-Division-Multiplexed CO-OFDM-OQAM System. *Optics and Photonics Journal*, **13**, 119-132.
https://doi.org/10.4236/opj.2023.136010

Received: March 15, 2023
Accepted: June 27, 2023
Published: June 30, 2023

Abstract

Contrary to the other multi-carrier modulation systems, the coherent optical orthogonal frequency division multiplexing communication system with an offset quadrature amplitude modulation (CO-OFDM-OQAM) possesses inherent imaginary interference (IMI). This has an important impact on the channel estimation process. Currently, a variety of frequency-domain channel estimation methods have been proposed. However, there are various problems that still exist. For instance, in order to reduce the influence of IMI, it is necessary to insert more guard intervals between the training sequence and the payload, leading to the occupation of excessive spectrum resources. In order to address this problem, this work designs a high spectral efficient frequency-domain channel estimation method for the polarization-division-multiplexing CO-OFDM-OQAM systems. First, the working principle of the proposed method is described in detail. Then, its spectral efficiency, power peak-to-average ratio, and channel estimation performance are studied based on simulations. The simulation results show that the proposed method improves the spectral efficiency without worsening the power peak-to-average ratio. The channel estimation capability of this method is verified in three scenarios of long-distance transmissions, including back-to-back, 100 km, and 200 km transmissions.

Keywords

Orthogonal Frequency Division Multiplexing (OFDM-OQAM), Polarization-Division-Multiplexing (PDM), Channel Estimation, Optical Communication System

1. Introduction

With the rapid development of communication technologies, multi-carrier modulation has been a focus of research community. Due to the use of pulse-shaping filters with good time-frequency characteristics, the orthogonal frequency division multiplexing communication system with an offset quadrature amplitude modulation (OFDM-OQAM) has lower out-of-band energy leakage and higher spectral efficiency [1] [2] [3]. The combination of coherent optical OFDM-OQAM and polarization-division-multiplexing (PDM CO-OFDM-OQAM) further improves the spectral efficiency and transmission capacity [4] [5] [6]. The channel estimation is a crucial signal processing step in any communication system. By obtaining accurate information regarding the channel response, the channel impairments can be effectively inversed. Contrary to the traditional OFDM, OFDM-OQAM only satisfies the orthogonality condition in the real domain and does not satisfy the orthogonality condition in the complex domain, resulting in an inherent imaginary interference (IMI) [7] [8]. This phenomenon affects the channel estimation process of the OFDM-OQAM systems. Therefore, the influence of IMI and polarization mode dispersion (PMD) should also be considered in addition to the influence of chromatic dispersion and noise, especially in case of PDM CO-OFDM-OQAM [9]. Consequently, the design of channel estimation algorithms is relatively difficult [10] [11]. François Horlin *et al.* discussed the feasibility of combining OFDM-OQAM and PDM to enhance the spectral efficiency [12]. Zhaohui Li *et al.* presented the experimental verification of PDM CO-OFDM-OQAM [13]. However, due to the influence of PMD and IMI, the channel equalization of PDM CO-OFDM-OQAM is quite different from other polarization division multiplexing systems [14] [15] [16]. François Horlin *et al.* designed a minimum mean square error (MMSE) time-domain equalizer for PDM CO-OFDM-OQAM [12]. Xi Fang *et al.* designed and studied a time-domain channel estimation method for PDM CO-OFDM-OQAM [17]. Nhat-Quang Nhan *et al.* redesigned a sparse pilot structure and used it to estimate the channel response of PDM CO-OFDM-OQAM [18]. Please note that the common problem in the three aforementioned methods is that they are all time-domain channel estimation schemes, which have high computational complexity. Few methods with lower computational complexity that perform channel estimation and equalization in the frequency domain are also presented. Xi Fang *et al.* proposed two frequency-domain channel estimation methods for PDM CO-OFDM-OQAM [19], using half-loaded and full-loaded pilots, respectively, for performing channel estimation. Under the same transmission conditions, the full-loaded method shows better channel equalization characteristics. In [20], Bangjiang Lin *et al.* applied the above two methods to PDM OFDM-OQAM for the intensity modulation-direct detection.

It is evident from the aforementioned analysis that the channel estimation methods of PDM CO-OFDM-OQAM are divided into two categories, *i.e.*, the time-domain methods and the frequency-domain methods. The time-domain methods have high computationally complexity and are difficult to use in prac-

tical environment. There are two frequency-domain methods, *i.e.*, half-loaded method and full-loaded method. Under the same transmission conditions, the full-loaded method shows better channel equalization characteristics. The traditional full-loaded methods either use the real pilot-based interference approximation training sequences (IAM-R) [19] or the complex pilot-based enhanced IAM (E-IAM-C) [18]. Please note that the frequency-domain channel estimation methods presented in literature suffer from two problems, including more null subcarriers need to be inserted to form the guard interval, and the spectral efficiency requires further improvement. The peak-to-average power ratio (PAPR) of the training sequence is ignored. In this work, a high spectral efficiency frequency-domain channel estimation method for PDM CO-OFDM-OQAM is designed. In the proposed method, a data frame is composed of a training sequence and a payload, and the training sequence for each polarization branch requires only four frequency-domain symbols. In contrast, other frequency-domain estimation methods require at least six frequency-domain symbols, thus the spectral efficiency is improved. The real-valued pilot is a random sequence, which does not make the PAPR of the signal worse. In order to verify the effectiveness of the proposed method, a numerical simulation platform for PDM CO-OFDM-OQAM is also designed in this work. Subsequently, its channel estimation performance in amplified spontaneous emission (ASE) noise channels and real optical fiber channels is studied. Finally, the channel estimation and equalization capabilities of different methods are compared. The experimental results show that the proposed method still has a very good channel equalization performance even for nonlinear optical fiber channels.

2. The Modulation and Demodulation Principle of PDM CO-OFDM-OQAM

Figure 1 shows the working principal diagram of PDM CO-OFDM-OQAM. We denote the baseband signals transmitted in the x-polarized and y-polarized states as $s_x(t)$ and $s_y(t)$, respectively. These signals are mathematically expressed as follows:

$$\begin{cases} s_x(t) = \sum_{n=1}^{N_s} \sum_{m=0}^{M-1} a_{x,m,n} g(t - n\tau_0) e^{j2\pi m f_0 \left(t - \frac{KM-1}{2} T_s\right)} e^{j\pi \frac{m+n-2mn}{2}} \\ s_y(t) = \sum_{n=1}^{N_s} \sum_{m=0}^{M-1} a_{y,m,n} g(t - n\tau_0) e^{j2\pi m f_0 \left(t - \frac{KM-1}{2} T_s\right)} e^{j\pi \frac{m+n-2mn}{2}} \end{cases}, \quad (1)$$

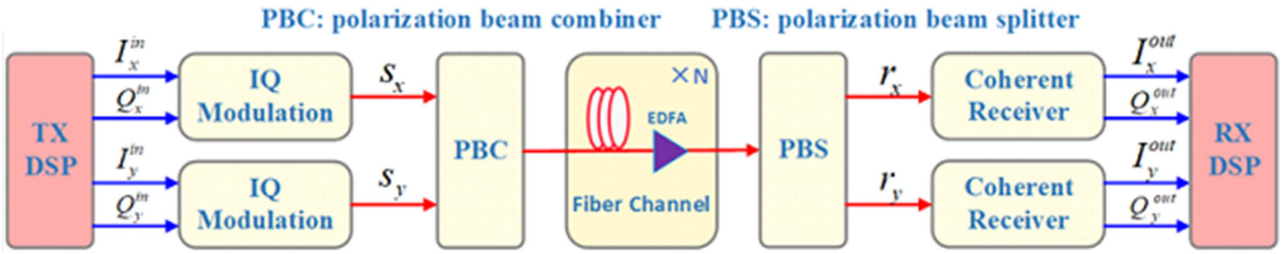

Figure 1. The working principal of PDM CO-OFDM-OQAM.

where, $g(t)$ represents the pulse-shaping filter, $a_{x,m,n}$ and $a_{y,m,n}$ represent the real-valued signals transmitted through the x and y polarized states at the time-frequency grid point (m,n). The total number of subcarriers is M, the interval between the adjacent subcarriers is $f_0 = 1/T$, and T represents the time duration of one OFDM-OQAM complex symbol. T_s represents the time-domain sampling interval and K represents the overlap factor of $g(t)$.

When the time-domain waveform passes through the optical fiber channel, it is affected by the dispersion, PMD, and ASE noise. This work uses h_{xx}, h_{yy}, h_{xy}, and h_{yx} to represent the channel impulse response of polarization division multiplexed optical fiber channel. Here, h_{xx} and h_{yy} represent the dispersion-induced impulse responses of the x-polarized and y-polarized states, respectively, h_{xy} represents the polarization crosstalk from the x-polarized state to the y-polarized state caused by the PMD, and h_{yx} represents the polarization crosstalk from the y-polarized state to the x-polarized state caused by the PMD. When the optical signal passes through the fiber channel, the received signal is mathematically expressed as follows:

$$\begin{bmatrix} r_x(t) \\ r_y(t) \end{bmatrix} = \begin{bmatrix} h_{xx} & h_{yx} \\ h_{xy} & h_{yy} \end{bmatrix} \otimes \begin{bmatrix} s_x(t) \\ s_y(t) \end{bmatrix} + \begin{bmatrix} w_x(t) \\ w_y(t) \end{bmatrix}. \tag{2}$$

In Equation (2), $w_x(t)$ and $w_y(t)$ represent the additive complex noises that are added in the transmitted signal in the x and y polarized states, respectively, and $\otimes$ denotes the convolution operation.

After photoelectric conversion, the received signal also needs to recover the data carried by the sub-carriers based on the analysis filter bank (AFB) and fast Fourier transform. Using the orthogonality condition in the real domain, the demodulated signal at (m,n) is obtained as follows:

$$\begin{aligned} r_{x,m,n} &= H_{xx,m,n}a_{x,m,n} + \sum_{(p,q)\neq(0,0)} H_{xx,m+p,n+q}a_{x,m+p,n+q}\zeta_{m,n}^{m+p,n+q} \\ &\quad + H_{yx,m,n}a_{y,m,n} + \sum_{(p,q)\neq(0,0)} H_{yx,m+p,n+q}a_{y,m+p,n+q}\zeta_{m,n}^{m+p,n+q}, \\ &\quad + W_{x,m,n} \end{aligned} \tag{3}$$

$$\begin{aligned} r_{y,m,n} &= H_{yy,m,n}a_{y,m,n} + \sum_{(p,q)\neq(0,0)} H_{yy,m+p,n+q}a_{y,m+p,n+q}\zeta_{m,n}^{m+p,n+q} \\ &\quad + H_{xy,m,n}a_{x,m,n} + \sum_{(p,q)\neq(0,0)} H_{xy,m+p,n+q}a_{x,m+p,n+q}\zeta_{m,n}^{m+p,n+q}, \\ &\quad + W_{y,m,n} \end{aligned} \tag{4}$$

where, $H_{xx,m,n}$, $H_{yy,m,n}$, $H_{xy,m,n}$, and $H_{yx,m,n}$ represent the Fourier transforms of h_{xx}, h_{yy}, h_{xy}, and h_{yx}, *i.e.*, the channel frequency responses. $\zeta_{m,n}^{m+p,n+q} = \langle g_{m,n}, g_{m+p,n+q} \rangle = \int_{-\infty}^{+\infty} g_{m,n}(t) g_{m+p,n+q}^{*}(t) dt$ represents the IMI coefficient. The fiber channel is a slow time-varying channel, and the following relationships are established: $H_{xx,m+p,n+q} \approx H_{xx,m,n}$, $H_{yy,m+p,n+q} \approx H_{yy,m,n}$, $H_{xy,m+p,n+q} \approx H_{xy,m,n}$, and $H_{yx,m+p,n+q} \approx H_{yx,m,n}$. At the same time, the parameters $a_{x,m,n}^{(i)}$ and $a_{y,m,n}^{(i)}$ are introduced to represent the IMI of the adjacent carrier data in the x and y branches at the time-frequency grid point (m,n), respectively, and are mathematically expressed as follows:

$$\begin{cases} a_{x,m,n}^{(i)} = \sum\limits_{(p,q)\in\Omega_{1.1}^{*}} a_{x,m+p,n+q} \left\langle g_{m,n}, g_{m+p,n+q} \right\rangle \\ a_{y,m,n}^{(i)} = \sum\limits_{(p,q)\in\Omega_{1.1}^{*}} a_{y,m+p,n+q} \left\langle g_{m,n}, g_{m+p,n+q} \right\rangle \end{cases}, \tag{5}$$

where, $\Omega_{(1.1)}^{*} = \Omega_{(1.1)} - (0,0)$ represents the first-order nearest neighbor region of the time-frequency grid point (m,n). Substituting Equation (5) into Equation (3) and Equation (4) and rewriting it into matrix form, we obtain:

$$\begin{bmatrix} r_{x,m,n} \\ r_{y,m,n} \end{bmatrix} = \begin{bmatrix} H_{xx,m,n} & H_{yx,m,n} \\ H_{xy,m,n} & H_{yy,m,n} \end{bmatrix} \begin{bmatrix} a_{x,m,n} + a_{x,m,n}^{(i)} \\ a_{y,m,n} + a_{y,m,n}^{(i)} \end{bmatrix} + \begin{bmatrix} W_{x,m,n} \\ W_{y,m,n} \end{bmatrix}. \tag{6}$$

It is evident from the aforementioned expression that in order to obtain the demodulation information from each subcarrier, the following operations are performed:

$$\begin{bmatrix} \hat{a}_{x,m,n} \\ \hat{a}_{y,m,n} \end{bmatrix} = \mathrm{Re}\left\{ \begin{bmatrix} h_{xx,m,n} & h_{yx,m,n} \\ h_{xy,m,n} & h_{yy,m,n} \end{bmatrix}^{-1} \begin{bmatrix} r_{x,m,n} \\ r_{y,m,n} \end{bmatrix} \right\}. \tag{7}$$

3. A High Spectral Efficient Frequency-Domain Channel Estimation Method

In order to further improve the spectral efficiency, this work proposes a frequency-domain channel estimation method with high spectral efficiency and low PAPR based on the modulation and demodulation principle of PDM CO-OFDM-OQAM. The flowchart of the process is presented in **Figure 2**. **Figure 3** shows the training sequence and the corresponding frame structure.

First, at the transmitter's end, the training sequence and the payload form a data frame, and a baseband transmission signal is generated based on this data frame. **Figure 3(a)** presents the training sequence of the proposed method. The training sequences of x-polarized and y-polarized states occupy four frequency-domain symbols, and the real-valued pilots are placed in the 2nd and 3rd frequency-domain symbols. The even-numbered sub-carriers of the x-polarized state are not zero, and all the odd-numbered sub-carriers are zero. On the contrary, the odd-numbered sub-carriers of the y-polarized state are not zero, and all the even-numbered sub-carriers are zero. Please note that the guard symbol is inserted before and after the real-valued pilots. The frame structure of the two polarization branches is shown in **Figure 3(b)**. For convenience, we denote the transmission training sequence in the x-polarized direction as $[z, p_{x1}, p_{x2}, z]$, and the transmission sequence in the y-polarized direction as $[z, p_{y1}, p_{y2}, z]$. These transmission sequences satisfy the following conditions:

$$p_{x1,2m,n} \neq 0, p_{x1,2m+1,n} = 0, p_{y1,2m,n} = 0, p_{y1,2m+1,n} \neq 0, \tag{8}$$

$$p_{x1,2m,n} = p_{x2,2m,n}, p_{y1,2m+1,n} = -p_{y2,2m+1,n}, \tag{9}$$

We use the superscripts (1) and (2) to represent the time positions of the two real-valued training symbols. Now, the received pilot signal is obtained according to Equation (6) as follows:

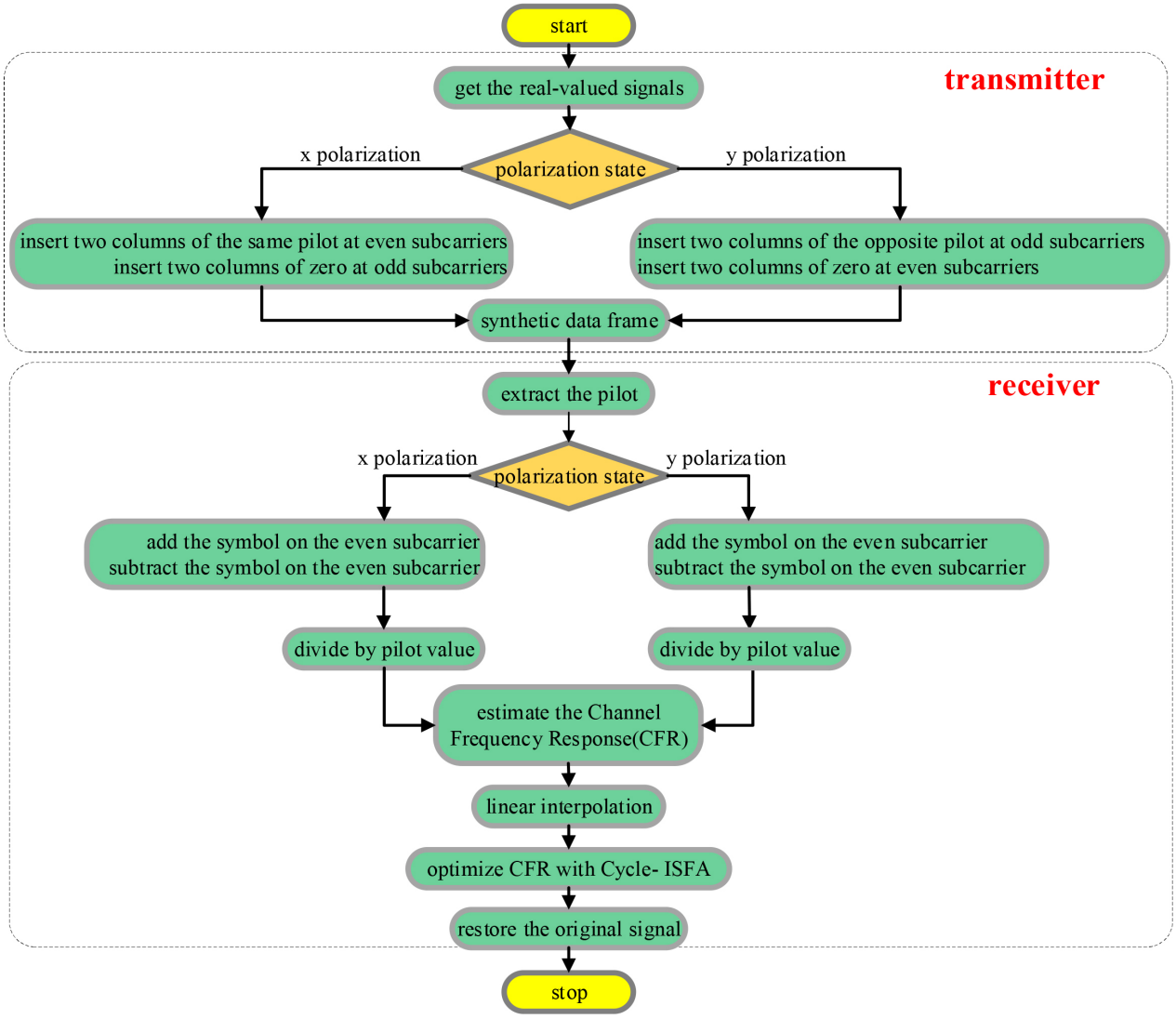

Figure 2. The flowchart of the method proposed in this work.

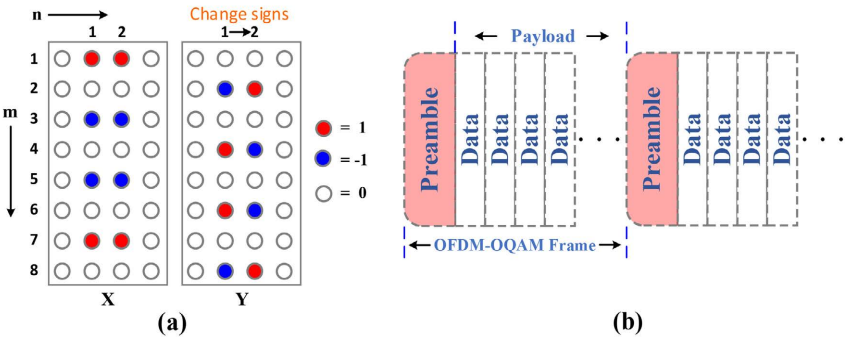

Figure 3. The pilot structure diagram of the method proposed in this work.

$$\begin{aligned} r_{x,m,n}^{(1)} &= H_{xx,m,n}\left(p_{x1,m,n}+p_{x1,m,n}^{(i)}\right)+H_{yx,m,n}\left(p_{y1,m,n}+p_{y1,m,n}^{(i)}\right)+w_x^{(1)} \\ r_{y,m,n}^{(1)} &= H_{xy,m,n}\left(p_{x1,m,n}+p_{x1,m,n}^{(i)}\right)+H_{yy,m,n}\left(p_{y1,m,n}+p_{y1,m,n}^{(i)}\right)+w_y^{(1)} \end{aligned}, \quad (10)$$

$$\begin{aligned} r_{x,m,n}^{(2)} &= H_{xx,m,n}\left(p_{x2,m,n}+p_{x2,m,n}^{(i)}\right)+H_{yx,m,n}\left(p_{y2,m,n}+p_{y2,m,n}^{(i)}\right)+w_x^{(2)} \\ r_{y,m,n}^{(2)} &= H_{xy,m,n}\left(p_{x2,m,n}+p_{x2,m,n}^{(i)}\right)+H_{yy,m,n}\left(p_{y2,m,n}+p_{y2,m,n}^{(i)}\right)+w_y^{(2)} \end{aligned}, \tag{11}$$

As discussed, the pilot frequencies $p_{x1}, p_{x2}, p_{y1}, p_{y2}$ satisfy the conditions presented in Equation (8) and Equation (9). Therefore, Equation (10) can be re-written as follows:

$$\begin{aligned} r_{x,2m,n}^{(1)} &= H_{xx,2m,n}\left(p_{x1,2m,n}+p_{x1,2m,n}^{(i)}\right)+H_{yx,m,n}\left(p_{y1,2m,n}^{(i)}\right) \\ r_{x,2m+1,n}^{(1)} &= H_{xx,2m+1,n}\left(p_{x1,2m+1,n}^{(i)}\right)+H_{yx,2m+1,n}\left(p_{y1,2m+1,n}+p_{y1,2m,n}^{(i)}\right) \\ r_{y,2m,n}^{(1)} &= H_{xy,2m,n}\left(p_{x1,2m,n}+p_{x1,2m,n}^{(i)}\right)+H_{yy,m,n}\left(p_{y1,2m,n}^{(i)}\right) \\ r_{y,2m+1,n}^{(1)} &= H_{xy,2m+1,n}\left(p_{x1,2m+1,n}^{(i)}\right)+H_{yy,2m+1,n}\left(p_{y1,2m+1,n}+p_{y1,2m,n}^{(i)}\right) \end{aligned}, \tag{12}$$

Similarly, Equation (11) can be rewritten as follows:

$$\begin{aligned} r_{x,2m,n}^{(2)} &= H_{xx,2m,n}\left(p_{x2,2m,n}+p_{x2,2m,n}^{(i)}\right)+H_{yx,m,n}\left(p_{y2,2m,n}^{(i)}\right) \\ r_{x,2m+1,n}^{(2)} &= H_{xx,2m+1,n}\left(p_{x2,2m+1,n}^{(i)}\right)+H_{yx,2m+1,n}\left(p_{y2,2m+1,n}+p_{y2,2m,n}^{(i)}\right) \\ r_{y,2m,n}^{(2)} &= H_{xy,2m,n}\left(p_{x2,2m,n}+p_{x2,2m,n}^{(i)}\right)+H_{yy,m,n}\left(p_{y2,2m,n}^{(i)}\right) \\ r_{y,2m+1,n}^{(2)} &= H_{xy,2m+1,n}\left(p_{x2,2m+1,n}^{(i)}\right)+H_{yy,2m+1,n}\left(p_{y2,2m+1,n}+p_{y2,2m,n}^{(i)}\right) \end{aligned}, \tag{13}$$

According to the modulation and demodulation principle of OFDM-OQAM, it can be proved that the pattern of IMI coefficient $\zeta_{m,n}^{m+p,n+q}$ has the following symmetry:

$$\begin{bmatrix} j(-1)^m\delta & -j\beta & j(-1)^m\delta \\ -j(-1)^m\gamma & a_{m,n} & j(-1)^m\gamma \\ j(-1)^m\delta & j\beta & j(-1)^m\delta \end{bmatrix}, \tag{14}$$

As discussed earlier, the real-valued pilots satisfy $p_{x1,2m,n} = p_{x2,2m,n}$, $p_{y1,2m+1,n} = -p_{y2,2m+1,n}$. Based on the symmetry of Equation (9) and Equation (14), it can be proved that the imaginary interference of real-valued pilot satisfies the following conditions:

$$p_{x1,2m,n}^{(i)} = -p_{x2,2m,n}^{(i)}, p_{x1,2m+1,n}^{(i)} = p_{x2,2m+1}^{(i)}, \tag{15}$$

$$p_{y1,2m,n}^{(i)} = -p_{y2,2m,n}^{(i)}, p_{y1,2m+1,n}^{(i)} = -p_{y2,2m+1}^{(i)}, \tag{16}$$

The following relationships are obtained by substituting Equation (15) and Equation (16) in Equation (12) and Equation (13):

$$r_{x,2m,n}^{(1)} + r_{x,2m,n}^{(2)} = H_{xx,2m,n}2p_{x1,2m,n}, \tag{17}$$

$$r_{x,2m+1,n}^{(1)} - r_{x,2m+1,n}^{(2)} = H_{yx,2m+1,n}2p_{y1,2m+1,n}, \tag{18}$$

$$r_{y,2m,n}^{(1)} + r_{y,2m,n}^{(2)} = H_{xy,2m,n}2p_{x1,2m,n}, \tag{19}$$

$$r_{y,2m+1,n}^{(1)} - r_{y,2m+1,n}^{(2)} = H_{yy,2m+1,n}2p_{y1,2m+1,n}, \tag{20}$$

It is evident from the aforementioned equations that the channel frequency response coefficient can be estimated by the following equations:

$$\begin{aligned} H_{xx,2m,n} &= \frac{r^{(1)}_{x,2m,n} + r^{(2)}_{x,2m,n}}{2p_{x1,2m,n}}, H_{yx,2m+1,n} = \frac{r^{(1)}_{x,2m+1,n} - r^{(2)}_{x,2m+1,n}}{2p_{y1,2m+1,n}} \\ H_{xy,2m,n} &= \frac{r^{(1)}_{y,2m,n} + r^{(2)}_{y,2m,n}}{2p_{x1,2m,n}}, H_{yy,2m+1,n} = \frac{r^{(1)}_{y,2m+1,n} - r^{(2)}_{y,2m+1,n}}{2p_{y1,2m+1,n}} \end{aligned}, \tag{21}$$

The channel response coefficients for other even and odd subcarrier positions are calculated by using the interpolation method.

Finally, in order to lessen the influence of noise and interference, this work uses intra-symbol frequency-domain average (ISFA) for further improving the channel estimation accuracy, *i.e.*, the ISFA channel estimation value of each frequency point is equal to the average of k points before and after this point. The channel frequency response after the ISFA is expressed as follows:

$$\left[h^{ML}_{m'}\right]_{ISFA} = \frac{\sum_{m=m'-k}^{m'+k}\left[h^{ML}_{m}\right]}{\min(m_{\max}, m'+k) - \max(m_{\min}, m'-k) + 1}, \tag{22}$$

where, $\left[h^{ML}_{m}\right]$ represents the least squares channel estimation value of the mth subcarrier. $m_{\max}$ and $m_{\min}$ represent the maximum and minimum number of effective subcarriers. The ISFA is repeated for the channel estimation values. After several cycles, the channel estimation accuracy is further improved. After the optimization of the channel frequency response is completed, the original information of all the payloads is recovered based on the operation presented in Equation (7).

4. Experimental Results and Discussion

In order to verify the channel estimation ability of the method proposed in this work, a numerical simulation platform for the CO-OFDM-OQAM communication system is built. The specific configuration is presented in **Figure 4**. The time-domain sampling rate of the system is set to 20 G samples/s. The total number of subcarriers (the size of the Fourier transform) is 512, the modulation format is 16-QAM, and the center frequency of the laser is 193.4 THz. At the transmitter's end, the binary bit sequences transmitted in the x and y polarized states are first generated. Then, two electrical signals are generated after the application of offset-QAM modulation, inverse fast inverse Fourier transform, and synthesis filter banks, respectively. The laser at the transmitting end generates two beams of orthogonal polarizations by using a polarization beam splitter and modulates the optical carrier with the x and y electrical signals in the Mach-Zehnder modulator, respectively, for generating the x and y polarized optical signals carrying the data. Then, these two signal lights are combined by the polarization beam combiner and transmitted via the optical fiber link. At the receiver's end, the received optical signal is first decomposed into two optical signals x and y by using the polarization beam splitter and after mixing with the beam

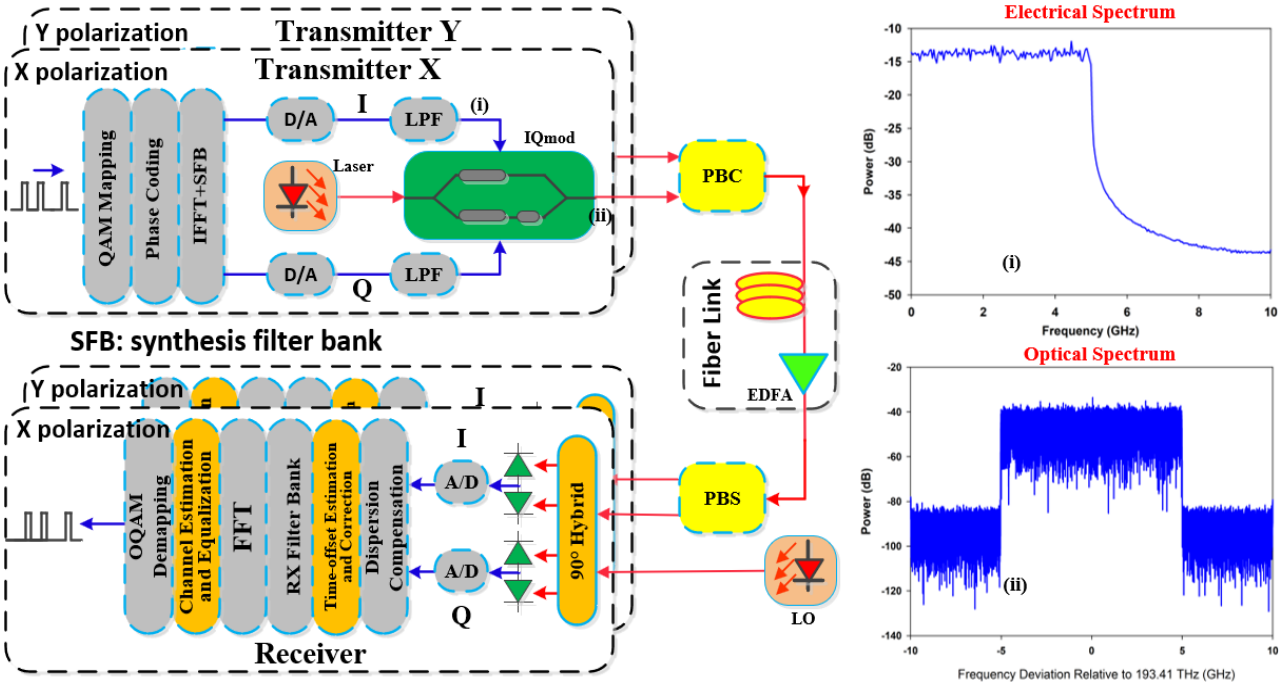

Figure 4. The numerical simulation configuration of PDM CO-OFDM-OQAM. The inset shows its electrical and optical spectrum. LO denotes the local oscillator laser and LPF denotes the low-pass filter.

emitted by the local oscillator laser, the signals enter the balanced detector for generating two electrical signals. The electrical domain digital signal processing includes AFB, Fourier transform, offset-QAM demodulation, channel response estimation and equalization. Finally, the binary bit sequence transmitted by the two branches is obtained and the bit error rate is computed.

In this work, we first calculate the PAPR values of PDM CO-OFDM-OQAM by using different channel estimation methods. These PAPR values are obtained by measuring the ratio of the peak power to the average power of the time-domain samples, and are mathematically expressed as follows:

$$R_{PAPR} = 10\log_{10}\left\{\frac{max[|s(t)|^2]}{E[|s(t)|^2]}\right\}, \tag{23}$$

where, $s(t)$ represents the sampling point of the transmission signal in time and $E[\cdot]$ represents the expectation operator. Since PAPR varies randomly between OFDM-OQAM symbols, a better metric for the multi-carrier signals is complementary cumulative distribution function (CCDF), *i.e.*, the probability when the PAPR exceeds a given threshold. If the threshold is expressed as T_h, the CCDF is expressed as $F_{CCDF} = 1 - Prob(R_{PAPR} \le T_h)$. The results obtained after averaging the x and y polarized states are shown in **Figure 5**. The figure clearly shows the change in the PAPR performance of the system before and after inserting the training sequences. The results show that E-IAM-C has the greatest impact on the PAPR performance of the system, whereas the proposed method has the least impact. The IAM-R method has almost the same impact on the system as the half-loaded method. The figure also shows the number of

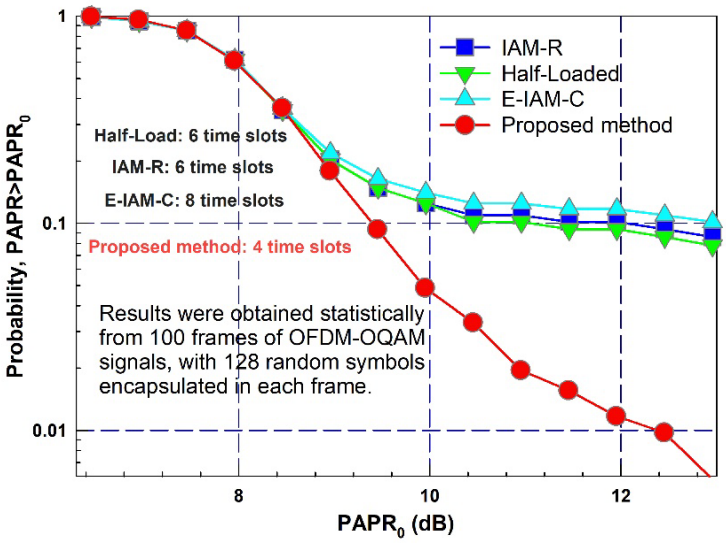

Figure 5. The complementary accumulation function used to represent the PAPR performance of different channel estimation methods for PDM CO-OFDM-OQAM.

frequency-domain symbols that the training sequence of each method needs to occupy. The training sequence on each polarization branch of the IAM-R method and the half-loaded method occupies six frequency-domain symbols, the E-IAM-C method occupies eight frequency-domain symbols, and the method proposed in this work only occupies four frequency-domain symbols.

Now, we investigate the channel estimation performance of the proposed method in back-to-back (BtB) case. The corresponding results are presented in **Figure 6**. The figure shows the correspondence between the system bit error rate (BER) and the OSNR. It is evident that in case of optical BtB, when the OSNR is less than 23 dB, the BER of this method after 6 cycles of ISFA is better than that of the IAM-R method. When the OSNR is less than 27 dB, the BER after 8 cycles of ISFA is better than that of the IAM-R method. In the OSNR range under investigation (10 dB - 30 dB), the BER of the proposed method after 10 cycles of ISFA is always better than that of the IAM-R method.

The channel estimation performance of the proposed method in this paper after 100 km and 200 km standard single-mode fiber (SSMF) transmission is shown in **Figure 7**. Please note that in this work, the fiber nonlinearity is not considered temporarily. The fiber dispersion coefficient is considered to be 16 ps/nm/km and the differential group delay (DGD) is set to 5 ps/km$^{1/2}$. In case of 100 km optical fiber transmission, when the OSNR is less than 23 dB, after 6 cycles of ISFA, the BER of the proposed method in this work is better than the IAM-R method. In the OSNR range of 12 dB to 25 dB, after 8 cycles of ISFA, the BER of the proposed method in this work is always better than that of the IAM-R method. If the fiber length is increased to 200 km, when the OSNR is less than 21.5 dB, the BER of the proposed method is better than that of the IAM-R method after 6 cycles of ISFA. When the OSNR is less than 22.5 dB, the BER after 8 cycles of ISFA is better than that of the IAM-R method.

An important difference between the fiber and wireless channels is the nonlinearity of the fiber, which can lead to physical impairments, such as self-phase modulation, cross-phase modulation, and four-wave mixing, etc. However, the authors in [16] [17] did not consider the nonlinearity of the fiber. In the previous stage of research, this work compared the channel estimation capabilities of different methods in the linear fiber channels by ignoring the nonlinearity of the fiber. The last part of this work focuses on the channel estimation performance of the proposed method in nonlinear fiber channels. **Figure 8** shows the correspondence between the BER and fiber input power after 100 km SSMF transmission. The damage caused by the nonlinearity of the fiber is described by the nonlinear refractive index (2.6×10^{-20} m^2/W). The EDFA introduces ASE noise with a noise index of 4 dB. The 7% hard-decision forward error correction code limit is marked with a dashed line in the figure and noted in text. The transmission of an optical signal in a dispersive and nonlinear SSMF was simulated by solving the coupled nonlinear Schrödinger equation using the split-step

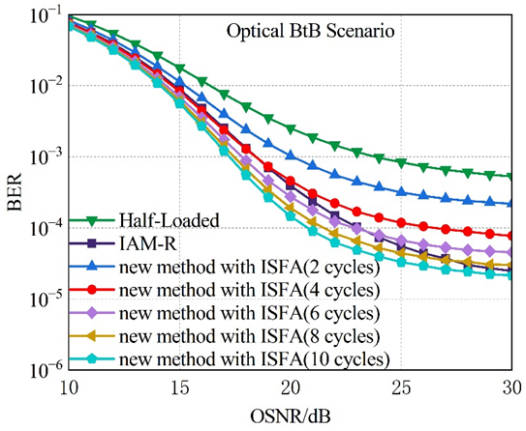

Figure 6. The BER performance of different channel estimation methods in the case of optical BtB.

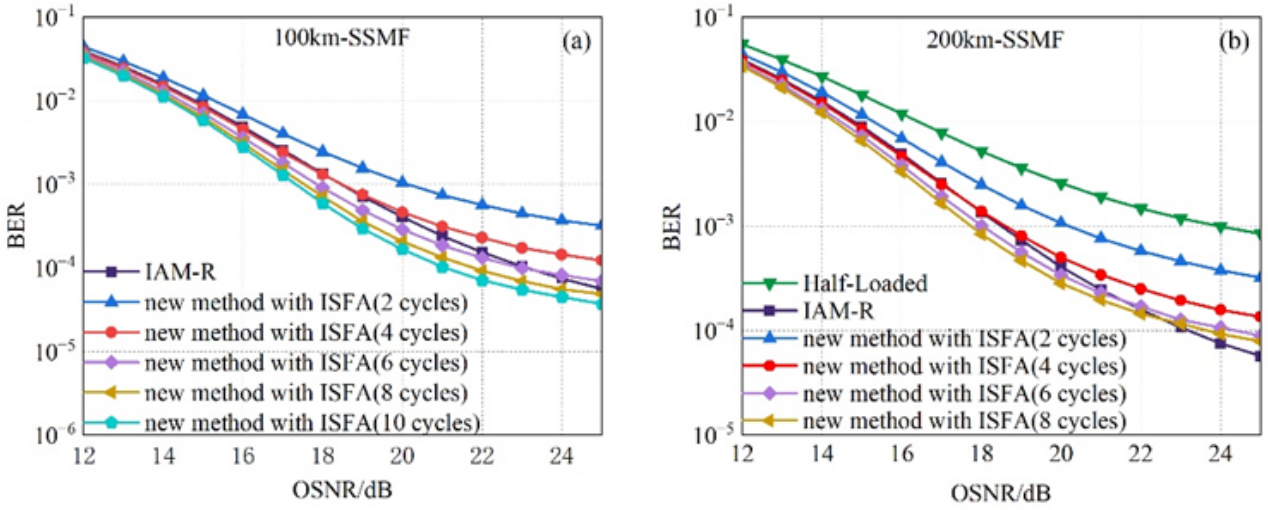

Figure 7. The BER performance under different channel estimation methods after SSMF transmission: (a) 100 km, (b) 200 km.

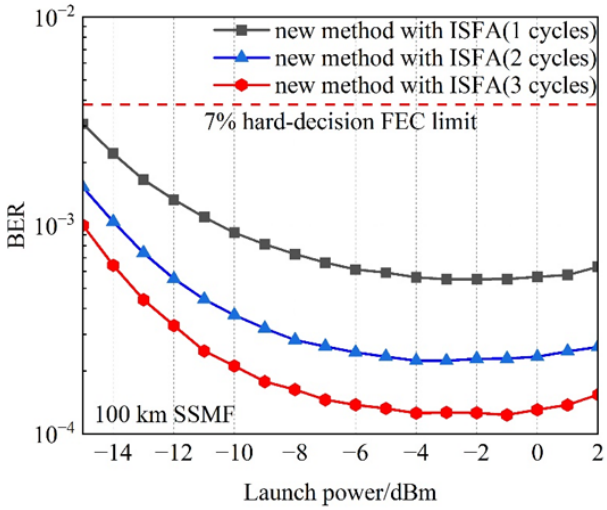

Figure 8. The bit error rate performance of the proposed method in this work for the nonlinear optical fiber channels.

Fourier method [21]. The nonlinear fiber channels generate two noises, including ASE noise and nonlinear interference. As shown in **Figure 8**, when the input power is relatively small, the received signal quality is mainly limited by the ASE noise. As the input power increases, the nonlinear interference begins to dominate and severely degrade the quality of the received signal. At the optimal input power, the BER is minimal. As the number of ISFA cycles increases from 1 to 3, the BER performance of the proposed method becomes better, and the corresponding optimized input powers are equal to: −2 dBm, −3 dBm, and −1 dBm, respectively. These results demonstrate that the proposed method provides efficient channel estimation capability in both linear and nonlinear fiber channels.

5. Conclusion

This work proposes and studies an improved frequency-domain channel estimation method for PDM CO-OFDM-OQAM systems. The main advantage of this method is that only four frequency-domain symbols are required for the training sequence of each polarization branch. As compared with the interference approximation method using real-valued pilots (IAM-R), the number of symbols occupied by the training sequence is reduced by 33.3%. As compared with the E-IAM-C method using complex pilots, the number of symbols occupied by the training sequence is reduced by 50%. This significantly improves the spectral efficiency. Moreover, in the proposed method, the real-valued pilot is a random sequence, which does not make the PAPR of the signal worse. The channel estimation capability of the proposed method is verified quantitively in an actual fiber channel by considering the effects of fiber dispersion, polarization mode dispersion, and nonlinearity. The results show that the proposed method achieves better BER performance even for nonlinear fiber channels. The method proposed in this work provides a useful reference for the research and development of short-distance fiber communication systems based on OFDM-OQAM.

Conflicts of Interest

The authors declare no conflicts of interest regarding the publication of this paper.

References

[1] Shieh, W., Yang, Q. and Ma, Y. (2008) 107 Gb/s Coherent Optical OFDM Transmission over 1000-km SSMF Fiber Using Orthogonal Band Multiplexing. *Optics Express*, **16**, 6378-6386. https://doi.org/10.1364/OE.16.006378

[2] Haider, F. (2014) Cellular Architecture and Key Technologies for 5G Wireless Communication Networks. *Journal of Chongqing University of Posts & Telecommunications*, **52**, 122-130. https://doi.org/10.1109/MCOM.2014.6736752

[3] Nissel, R., Schwarz, S. and Rupp, M. (2017) Filter Bank Multicarrier Modulation Schemes for Future Mobile Communications. *IEEE Journal on Selected Areas in Communications*, **35**, 1768-1782. https://doi.org/10.1109/JSAC.2017.2710022

[4] Siohan, P., Siclet, C. and Lacaille, N. (2002) Analysis and Design of OFDM/OQAM Systems Based on Filterbank Theory. *IEEE Transactions on Signal Processing*, **50**, 1170-1183. https://doi.org/10.1109/78.995073

[5] Nedic, S. (2000) An Approach to Data-Driven Echo Cancellation in OQAM-Based Multicarrier Data Transmission. *IEEE Transactions on Communications*, **48**, 1077-1082. https://doi.org/10.1109/26.855512

[6] Floch, B.L., Alard, M. and Berrou, C. (1995) Coded Orthogonal Frequency Division Multiplex [TV Broadcasting]. *Proceedings of the IEEE*, **83**, 982-996. https://doi.org/10.1109/5.387096

[7] Liu, J.J., Wang, D.B., Tuo, M.S., Wang, W., Yuan, L.H., Cao, M.H. and Wang, H.Q. (2020) Joint Estimation Algorithm of Time Offset and Channel Response for Coherent Optical FBMC-OQAM Systems. *Chinese Journal of Lasers*, **47**, Article 1106001. https://doi.org/10.3788/CJL202047.1106001

[8] Chong, H.D., Wang, D.B., Yuan, L.H., Li, X.X., Cao, M.H. and Wang, H.Q. (2019) Estimation and Compensation of Integer Frequency Offset in Coherent Optical Offset Quadrature Amplitude Modulation Based Filter Bank Multicarrier Systems. *Acta Optica Sinica*, **39**, 9. https://doi.org/10.3788/AOS201939.1206008

[9] Yeh, C.H., Hsu, W.H., Wang, B.Y., Chen, J.R., You, W.Y. and Chow, C.W. (2021) Dual-Polarized WDM Access Network with Fiber to the Extension (FTTE) Connection. *IEEE Photonics Journal*, **13**, 1-6. https://doi.org/10.1109/JPHOT.2021.3087901

[10] Ibragimov, E. and Schmidt, T.J. (2011) Polarization Monitoring in Polarization Division Multiplexing in Optical Communications. Google Patents.

[11] Shieh, W., Yi, X., Ma, Y. and Tang, Y. (2007) Theoretical and Experimental Study on PMD-Supported Transmission Using Polarization Diversity in Coherent Optical OFDM Systems. *Optics Express*, **15**, 9936-9947. https://doi.org/10.1364/OE.15.009936

[12] Horlin, F., Fickers, J., Emplit, P., Bourdoux, A. and Louveaux, J. (2013) Dual-Polarization OFDM-OQAM for Communications over Optical Fibers with Coherent Detection. *Optics Express*, **21**, 6409-6421. https://doi.org/10.1364/OE.21.006409

[13] Li, Z., Jiang, T., Li, H.. Zhang, X., Li, C., Li, C., Hu, R., Luo, M., Zhang, X. and Xiao, X. (2013) Experimental Demonstration of 110-Gb/s Unsynchronized Band-Multiplexed Superchannel Coherent Optical OFDM/OQAM System. *Optics Express*, **21**, 21924-21931. https://doi.org/10.1364/OE.21.021924

[14] Yao, X.S., Yan, L.S., Zhang, B., Willner, A.E. and Jiang, J. (2007) All-Optic Scheme for Automatic Polarization Division Demultiplexing. *Optics Express*, **15**, 7407. https://doi.org/10.1364/OE.15.007407

[15] Stuart, H.R. (2000) Dispersive Multiplexing in Multimode Fiber. *Science*, **289**, 281. https://doi.org/10.1126/science.289.5477.281

[16] Cheng, Y., Tan, J., Liu, L., He, J., Tang, J., Chen, L., Zhang, J., Li, Q. and Xiao, M. (2016) Method of Joint Frame Synchronization and Data-Aided Channel Estimation for 100-Gb/s Polarization-Division Multiplexing-Single Carrier Frequency Domain Equalization Coherent Optical Transmission Systems. *Optical Engineering*, **55**, Article 026118. https://doi.org/10.1117/1.OE.55.2.026118

[17] Fang, X., Xu, Y., Chen, Z. and Zhang, F. (2016) Time-Domain Least Square Channel Estimation for Polarization-Division-Multiplexed CO-OFDM/OQAM Systems. *Journal of Lightwave Technology*, **34**, 891-900. https://doi.org/10.1109/JLT.2015.2507605

[18] Nhan, N.Q., Morel, P., Azou, S., Morvan, M., Gravey, P. and Pincemin, E. (2018) Sparse Preamble Design for Polarization Division Multiplexed CO-OFDM/OQAM Channel Estimation. *Journal of Lightwave Technology*, **36**, 2737-2745. https://doi.org/10.1109/JLT.2018.2822732

[19] Fang, X., Xu, Y., Chen, Z. and Zhang, F. (2015) Frequency-Domain Channel Estimation for Polarization-Division-Multiplexed CO-OFDM/OQAM Systems. *Journal of Lightwave Technology*, **33**, 2743-2750. https://doi.org/10.1109/JLT.2015.2410281

[20] Lin, B., Fang, X., Tang, X., Lin, C., Li, Y., Zhang, S., Wu, Y. and Li, H. (2016) Efficient Frequency-Domain Channel Equalization Methods for Dual-Polarization Orthogonal Frequency-Division Multiplexing/Offset Quadrature Amplitude Modulation-Passive Optical Network. *Optical Engineering*, **55**, Article 106108. https://doi.org/10.1117/1.OE.55.10.106108

[21] Sasai, T., Nakamura, M., Yamazaki, E., Yamamoto, S., Nishizawa, H. and Kisaka, Y. (2022) Digital Longitudinal Monitoring of Optical Fiber Communication Link. *Journal of Lightwave Technology*, **40**, 2390-2408. https://doi.org/10.1109/JLT.2021.3139167